Remote Sensing of Environment 180 (2016) 418–430

Contents lists available at ScienceDirect

Remote Sensing of Environment

journal homepage: www.elsevier.com/locate/rse

Spatial and temporal scales of variability in Tropical Atlantic sea surface salinity from the SMOS and Aquarius satellite missions

Eleni Tzortzi *, Meric Srokosz, Christine Gommenginger, Simon A. Josey

National Oceanography Centre, European Way, SO14 3ZH, Southampton, United Kingdom

ARTICLE INFO

Article history:
Received 23 July 2015
Received in revised form 21 December 2015
Accepted 2 February 2016
Available online 22 February 2016

Keywords:
Sea surface salinity variability
spatial and temporal decorrelation length scales
SMOS
Aquarius
Tropical Atlantic

ABSTRACT

Taking advantage of the spatially dense, multi-year time series of global Sea Surface Salinity (SSS) from two concurrent satellite missions, the spatial and temporal decorrelation scales of SSS in the Tropical Atlantic 30°N–30°S are quantified for the first time from SMOS and Aquarius observations. Given the dominance of the seasonal cycle in SSS variability in the region, the length scales are calculated both for the mean and anomaly (i.e. seasonal cycle removed) SSS fields. Different 7–10 days composite SSS products from the two missions are examined to explore the possible effects of varying resolution, bias corrections and averaging characteristics. With the seasonal cycle retained, the SSS field is characterized by strongly anisotropic spatial variability. Homogeneous SSS variations in the Tropics have the longest zonal scales of over ~2000 km and long temporal scales of up to ~70–80 days, as shown by both SMOS and Aquarius. The longest meridional scales, reaching over ~1000 km, are seen in the South Atlantic between ~10°–25°S, most discernible in Aquarius data. The longest temporal scales of SSS variability are reported by both satellites to occur in the North-West Atlantic region 15°–30°N, at the Southern end of the Sargasso Sea, with SSS persisting for up to 150–200 days. The removal of the seasonal cycle results in a noticeable decrease in the spatio-temporal decorrelation scales over most of the basin. Overall, with the exception of the differences in the South Atlantic, there is general agreement between the spatial and temporal scales of SSS from the two satellites and different products, despite differences in individual product calibration and resolution characteristics. These new estimates of spatio-temporal decorrelation scales of SSS improve our knowledge of the processes and mechanisms controlling the Tropical Atlantic SSS variability, and provide valuable information for a wide range of oceanographic and modelling applications.

1. Introduction

The characteristic decorrelation scales of ocean variables provide essential information about their spatial and temporal variability, evolution patterns, and the associated processes and controlling mechanisms. The variability in sea surface salinity (SSS) ranges from daily to annual and inter-annual scales and from sub-mesoscale (<10 km) to basin and global scales, responding to processes as diverse as intense precipitation events, river plumes meandering, advection by eddies and currents, and large-scale changes in atmospheric forcing e.g. Inter Tropical Convergence Zone (ITCZ) shift, ENSO teleconnection, etc. Among other processes, salinity-induced stratification at lower latitudes can also control the mixed layer depth through barrier layer effects (e.g. Lukas & Lindstrom, 1991), and therefore potentially regulate heat, gas and momentum exchanges between the ocean and the atmosphere. SSS is thus a useful proxy to monitor changes in the global hydrological cycle relevant to future climate variability (e.g. Schmitt, 2008), and to identify changes in the global ocean circulation and associated changes in ocean density distribution.

Over the last 5 years, a revolution in observing SSS from space has taken place, with several satellite missions concurrently in orbit: the first-ever satellite salinity mission, the European Space Agency Soil Moisture and Ocean Salinity (SMOS, e.g. Kerr et al., 2010; Mecklenburg et al., 2012), has been providing global maps of SSS continuously every 3 days since 2009; the US/Argentina Aquarius/SAC-D (Lagerloef et al., 2008) mission had been operational since 2011 but ceased functioning in early June 2015; and the NASA Soil Moisture Active Passive (SMAP, e.g. Brown et al., 2013) mission, launched on 31 January 2015, which, notwithstanding its main focus on soil moisture, should nevertheless deliver SSS products in due course. While satellite SSS measurements correspond to only the first few cm of the sea surface, they compare favourably with in situ surface salinity data from ships and Argo profiling floats measured typically at 5–10 m depth, except in regions of strong vertical salinity stratification such as precipitation bands in the Tropics and near river outflow and sharp oceanic fronts (e.g. Henocq et al., 2010; Boutin, Martin, Reverdin, Yin, & Gaillard, 2013). Validation studies against in situ observations reveal overall an accuracy of the order of ~0.3 pss for both SMOS (e.g. Boutin

* Corresponding author.
E-mail address: eltzortzi@gmail.com (E. Tzortzi).

http://dx.doi.org/10.1016/j.rse.2016.02.008

et al., 2012; Reul et al., 2012b; Banks, Gommenginger, Srokosz, & Snaith, 2012; Reul et al., 2013; Hernandez et al., 2014) and Aquarius (e.g. Lagerloef et al., 2013; Tang, Yueh, Fore, & Hayashi, 2014). Despite the relatively short time series of satellite SSS observations, numerous oceanographic studies have demonstrated the value of satellite SSS in providing a better description of key processes of the marine hydrological cycle, the mixed layer salinity budget and ocean circulation, among others (e.g. Lee et al., 2012; Hasson, Delcroix, & Boutin, 2013; Reul et al., 2013; Tzortzi, Josey, Srokosz, & Gommenginger, 2013; Boutin et al., 2014; Menezes, Vianna, & Phillips, 2014).

In this work, we take advantage of the availability of three full years (2012–2014) of concurrent global SSS measurements from SMOS and Aquarius to determine for the first time the characteristic spatial and temporal decorrelation scales of SSS from satellite data. Our results are discussed in the context of previous observation-based attempts to estimate SSS variability (e.g. Delcroix, McPhaden, Dessier, & Gouriou, 2005; Reverdin, Kestenare, Frankignoul, & Delcroix, 2007), which were necessarily constrained by the more limited coverage of in situ measurements from ships and floats. The focus of this paper is on the SSS variability in the Tropical Atlantic basin 30°N–30°S, including a small part of the Subtropics that falls within the domain considered here, in view of the important role of the region for the Atlantic Meridional Overturning Circulation (MOC, e.g. Vellinga & Wu, 2004) and its relevance to European weather and climate forecasting on seasonal to decadal time scales (e.g. Van den Dool et al., 2006). There has been increasing interest recently in assessing the value of satellite SSS data to improve predictions and ocean state estimates (Vernieres et al., 2014; Hackert, Busalacchi, & Ballabrera-Poy, 2014; Vinogradova, Ponte, Fukumori, & Wang, 2014; Köhl, Martins, & Stammer, 2014). Information on the decorrelation scales of SSS is also relevant to improve the development of gridded Level 3 (L3) SSS products from single-pass Level 2 (L2) data (e.g. Melnichenko, Hacker, Maximenko, Lagerloef, & Potemra, 2014) and for the production of Level 4 (L4) products where satellite SSS data are merged with other salinity observations (e.g. Hoareau, Umbert, Martínez, Turiel, & Ballabrera-Poy, 2014).

This paper is organized as follows: Section 2 describes the SMOS and Aquarius SSS datasets used in this work and the methodology for the calculation of the spatial and temporal scales. Section 3 presents the results for the spatial and temporal scales, followed by the discussion in Section 4. A summary and overall conclusions are given in Section 5.

2. Datasets and method

In this work, the decorrelation scales of satellite SSS in space and time are quantified from four different satellite SSS L3 and L4 products from the SMOS and Aquarius missions. Given the different launch dates of SMOS and Aquarius, the analysis is performed over the common period 2012–2014 for all datasets to enable direct comparisons of the estimated SSS variability. The four different satellite SSS products differ slightly in spatio-temporal resolutions, but more significantly, in the individual calibration and averaging strategies used to construct the L3 and L4 products. Other products are available (e.g. Melnichenko et al., 2014), but it is not practicable to analyse all the extant SMOS and Aquarius SSS products.

SMOS SSS L3 and L4 products over 2012–2014 at 0.5° × 0.5° spatial resolution are obtained from the Centre Aval de Traitement des Données SMOS Expertise Center-Ocean Salinity (CATDS-CECOS, www.catds.fr). L3 correspond to the 10-day Ifremer "research" L3 Version 2 (V2) products (Reul & Ifremer CATDS-CECOS Team, 2012; hereafter "Ifremer L3") and L4 correspond to the recently issued 7-day Ifremer L4 SSS products (Reul & Tenerelli, 2015; hereafter "Ifremer L4"). Apart from the minor difference in averaging period (7 days versus 10 days, a difference we assume negligible in the first instance), the main difference between the two SMOS Ifremer products regards the large-scale SSS bias correction. Specifically, the L3 V2 SSS products are bias-corrected based on the long-term average World Ocean Atlas 2001 (WOA01) climatology, while the L4 products are calibrated based on the inter-annually varying In Situ Analysis System (ISAS) climatology. In both cases, the bias-correction is applied with a 10° × 10° spatial running window (Reul & Tenerelli, 2015).

Our analyses are also applied to two Aquarius products with 1.0° × 1.0° spatial resolution in order to examine possible differences from the SSS variability reported by SMOS. Unfortunately, finer spatial resolution products are not available for Aquarius, mostly because of its sparser space–time sampling. The Aquarius data consist of the 7-day L3 Standard Mapped Image V3.0 products (Wentz, Yueh, & Lagerloef, 2014; hereafter "Aquarius SMI L3") obtained from the Physical Oceanography Distributed Active Archive Center (PODAAC), and the daily Aquarius Combined Active Passive with rain correction (CAP-RC) L3 V3.0 SSS products (Yueh & Chaubell, 2012; Yueh et al., 2013; Yueh, Tang, Fore, Hayashi, & Song, 2014; hereafter "Aquarius CAP-RC L3") obtained from the NASA Jet Propulsion Laboratory PODAAC. The daily CAP-RC L3 products are composites obtained over 7 days, and are provided after optimal interpolation (OI) using Gaussian weighting with half-power and searching distances of 75 km and 111 km respectively. Thus, the OI operates within the spatial resolution of the products with no impact on the scales estimates. For our analysis, the daily Aquarius CAP-RC data are simply sampled every 7 days in order to obtain weekly maps. The Aquarius data are calibrated using the HYbrid Coordinate Ocean Model (HYCOM) SSS in order to remove the global radiometer bias (Lagerloef et al., 2013; Yueh et al., 2014; Tang et al., 2014; Tang, Yueh, Fore, Hayashi, Lee and Lagerloef, 2014).

For the estimation of the spatial decorrelation scales of SSS, maps of SSS correlation are obtained by calculating the correlation coefficient, r, between the 3-year time-series of SSS in each target grid cell and all other grid cells in the Atlantic basin 30°N–30°S. The interest is in the homogeneous (in space or time) SSS changes, i.e. in-phase variations relative to a target grid point, which are defined here as those corresponding to positively correlated SSS patterns ($0 \geq r \geq 1$) around the target grid cell. An e-folding threshold is applied to the first occurrence below it to determine the length of the SSS characteristic spatial scales, i.e. the limit of the spatial feature with $r \geq 1 / e$ extending from the target grid cell to the North, South, West and East direction, respectively.

Examination of the spatial distribution of the correlation coefficient in the zonal and meridional direction, and maps of computed length scales of SSS in km in the 4-directions (N, S, W, E) indicated N–S and W–E symmetry around the target grid point (Tzortzi, 2015). This symmetry allows the calculation of the average W–E, i.e. zonal, and average N–S, i.e. meridional, spatial decorrelation scales. Likewise, the temporal decorrelation scales of SSS are determined by calculating the lagged auto-correlation of SSS in each target grid cell of the weekly or 10-day SSS product over the 3 years. As for the spatial scales, an e-folding threshold is applied to define the temporal decorrelation scales of SSS in each grid point.

Given the dominance of the seasonal cycle for the SSS variability in the Tropical Atlantic basin (e.g. Foltz & McPhaden, 2008), the estimation of the spatial and temporal decorrelation scales is performed both for the SSS mean field and the anomaly field. The SSS anomaly field is calculated by removing the seasonal cycle as characterized from the 7- or 10-day average value over the 3-year time series of SMOS or Aquarius data.

3. Results

3.1. Spatial decorrelation scales of SSS

In this section, spatial length scales derived from the various SMOS and Aquarius datasets with the seasonal cycle retained are considered. Here, the data are referred to as the 'mean' field to distinguish them from the 'anomaly' field with the seasonal cycle removed that is considered subsequently.

The zonal length scales of the SSS mean field obtained in the Atlantic basin 30°N–30°S for all four datasets are shown in Fig. 1. Overall, SMOS and Aquarius show similar, coherent spatial decorrelation scale fields, spanning most of the width of the basin. Homogeneous SSS variations occur over large zonal distances in the Tropics, particularly in three noticeable bands centred at 10°N, at the Eastern end of the Equatorial region and south of the Equator centred around ~5°S, all with decorrelation lengths that exceed 2000 km. Aquarius indicates, in general, slightly larger zonal scales in the Tropics than SMOS, that reach up to ~2700 km and ~2300 km for the SMI and CAP-RC products. For Aquarius, large zonal spatial scales comparable to those observed in the Tropics also dominate most of the South Atlantic between 10°-20°S, in contrast to SMOS, which shows shorter zonal scales that do not exceed 1000–1200 km and cover a smaller area (Fig. 1, a and b). Zonal decorrelation length scales of the order of 1000–1200 km are also detected at the southern end of the Sargasso Sea in the North-Western Atlantic (~20°–30°N), a feature that is clearly visible in all products except the Ifremer L3 data (Fig. 1, b–d).

The meridional spatial decorrelation length scales (Fig. 2) are noticeably shorter than the zonal scales, indicating strongly anisotropic spatial scales of mean SSS over the Tropical Atlantic basin, reported by both the SMOS and Aquarius products. Note the shorter color bar range of up to 1000 km in Fig. 2, compared to Fig. 1, where it reaches up to 2000 km. This anisotropy is clearly visible in the ratio of the zonal to meridional length scales of SSS shown in Fig. 3, which highlights that the zonal length scales can exceed the meridional length scales along the Tropics by up to a factor of 8. The zonal/meridional ratio decreases towards the Subtropics, reaching a factor of ~3, with further reduction in anisotropy over the rest of the basin and towards the coasts.

Over the basin, typical meridional length scales reach up to ~700 km from SMOS and ~1100 km from Aquarius (Fig. 2). As for the zonal scales (Fig. 1c and d), Aquarius generally provides larger meridional length scales than SMOS, particularly in the southern basin, where Aquarius meridional scales reach ~1300 km and dominate most of the region between 10° and 30°S (Fig. 2c and d). In the same area, SMOS indicates much shorter meridional length scales, except along two meridional bands centred at ~20°W and 0°E. All 4 datasets show meridional SSS lengths up to ~600–800 km in the Caribbean Current region (~15°N, 55°W). In the Southern Sargasso Sea, a similar feature to that seen in the zonal direction is observed again in all products except Ifremer L3 (Fig. 2b–d). Meridional scales also pick out features near the Guinea Dome (10°N, 20°W) not clearly seen in the zonal scales, and in the vicinity of the Angola Current and the Angola Dome (15°S, 0°E).

The information on zonal and meridional spatial scales of the SSS mean field from all 4 datasets is summarized in Fig. 4 in the form of zonal averages. The figure illustrates the good agreement between all

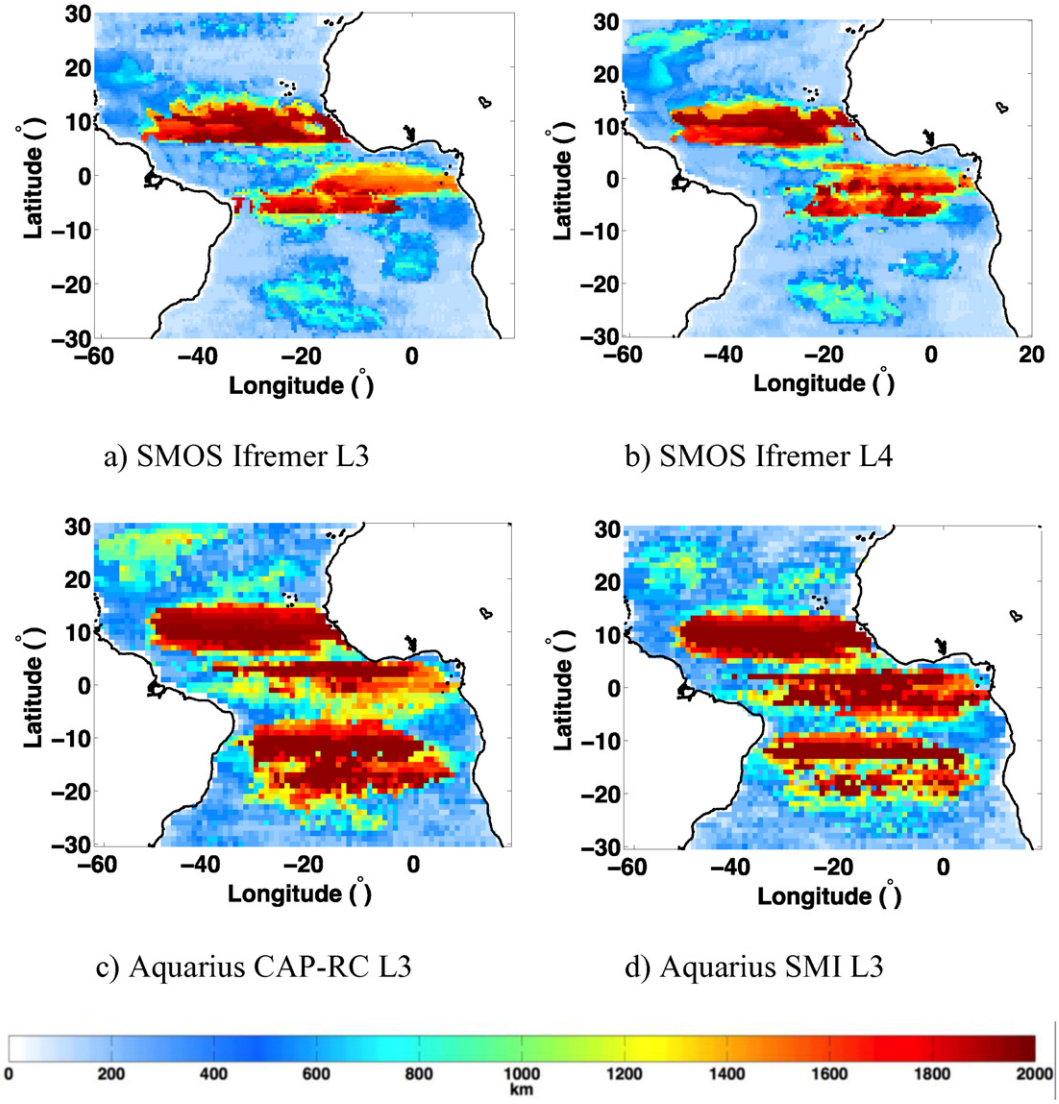

Fig. 1. The zonal spatial decorrelation scales of SSS mean field (in km), derived from the a) SMOS Ifremer L3, b) SMOS Ifremer L4, c) Aquarius CAP-RC L3 and d) Aquarius SMI L3 products.

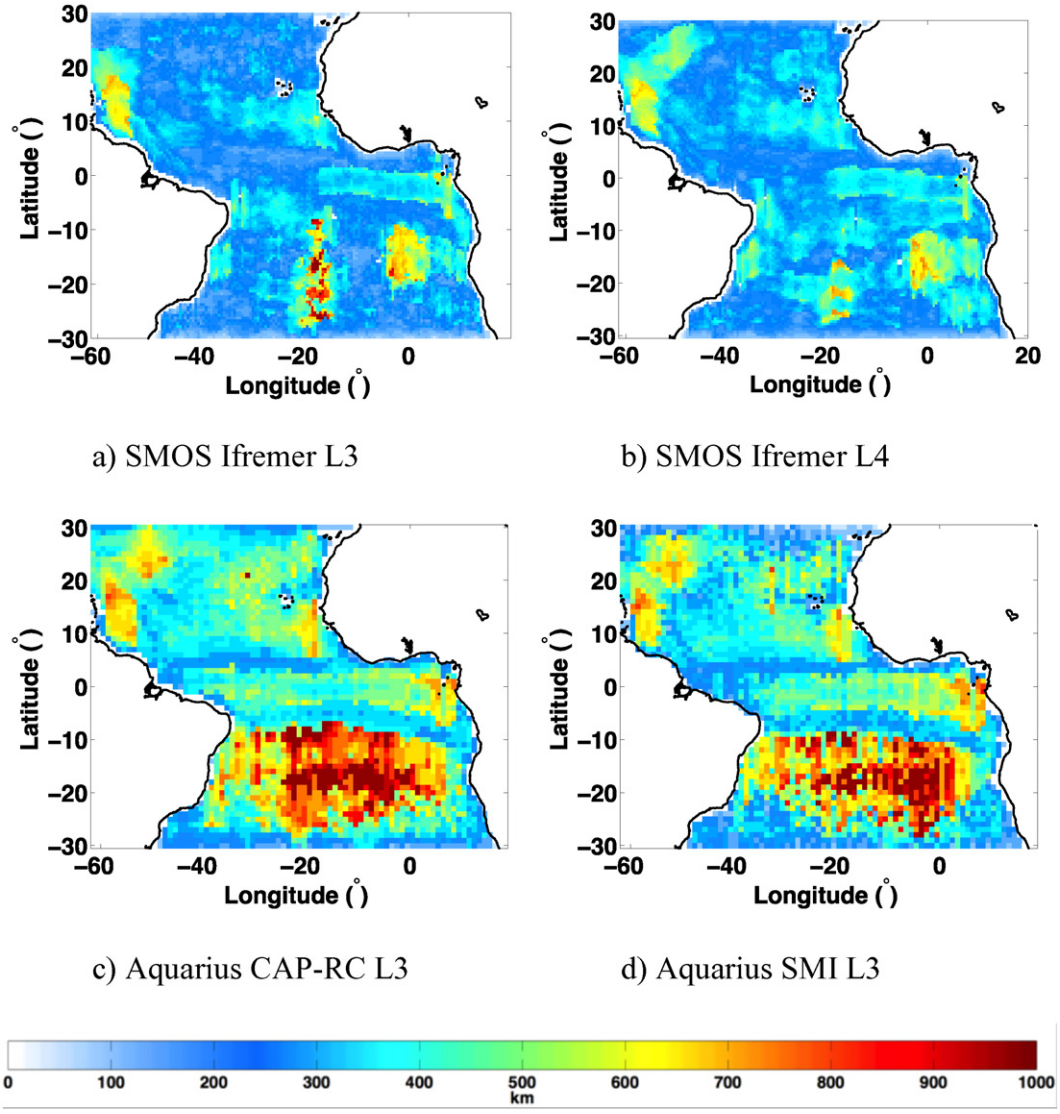

Fig. 2. The meridional spatial decorrelation scales of SSS mean field (in km), derived from the a) SMOS Ifremer L3, b) SMOS Ifremer L4, c) Aquarius CAP-RC L3 and d) Aquarius SMI L3 products. Note the shorter color bar range (up to 1000 km) compared to Fig. 1 (up to 2000 km).

SMOS and Aquarius products regarding the magnitude and position of zonal decorrelation scales in the North Tropical Atlantic around ~10°N (Fig. 4a). However, the agreement in the rest of the basin is poor: SMOS L3 and L4 products place a second smaller double-peak southwards of the Equator centred around ~5°S, while Aquarius SMI and CAP-RC suggest a larger double-peak centred at the Equator. Interestingly, Aquarius SMI shows an overall maximum slightly south of the Equator that is not evident from the CAP-RC dataset, possibly due to the rain correction applied to the latter. Finally, as reported already, considerably larger zonal scales are observed for both Aquarius products around 10°–20°S, which are not seen in either SMOS datasets.

This is also the case for the zonally averaged meridional scales (Fig. 4b), with Aquarius showing generally larger scales than SMOS, particularly in the band 10°S–25°S. Elsewhere, SMOS and Aquarius show reasonably good agreement for the shortest meridional spatial lengths, particularly in a narrow band at 5°N which also displays very short zonal scales (Fig. 4a). It is possible that the combined influence of SSS controlling mechanisms such as the ITCZ-driven precipitation patterns, strong zonal currents and equatorial upwelling prevent coherent SSS variations from occurring over long spatial scales in this dynamic band.

3.2. Spatial decorrelation scales of SSS anomaly

Spatial decorrelation scales obtained from SMOS and Aquarius SSS with the seasonal cycle removed are now examined. The removal of the seasonal cycle results in a significant decrease of the zonal spatial scales (Fig. 5) and of the meridional scales (Fig. 6), which now only reach up to ~1000 km and ~600 km, respectively. Anisotropy of the spatial decorrelation length scales is retained for the SSS anomaly field, but with smaller magnitude and over much smaller regions (Fig. 7; note the shorter color bar range relative to Fig. 3). The anisotropy persists particularly in the Northern Tropics and the Eastern Equatorial basin, where the ratio of zonal/meridional scales reaches values up to 4 in all four datasets. These nevertheless contrast strongly with the values of anisotropy up to 8 previously observed for the mean SSS field (Fig. 3). Elsewhere, the spatial scales of SSS anomalies are close to isotropic (Fig. 7).

The patterns of anisotropy in Fig. 7 can be traced back to larger decorrelation length scales in the same regions in the zonal direction (Fig. 5), where SSS anomalies continue to span very long distances over the N. Tropical and Eastern Equatorial Atlantic. As before, the Aquarius products, particularly the CAP-RC, report slightly longer zonal length scales and over larger regions than SMOS, including some

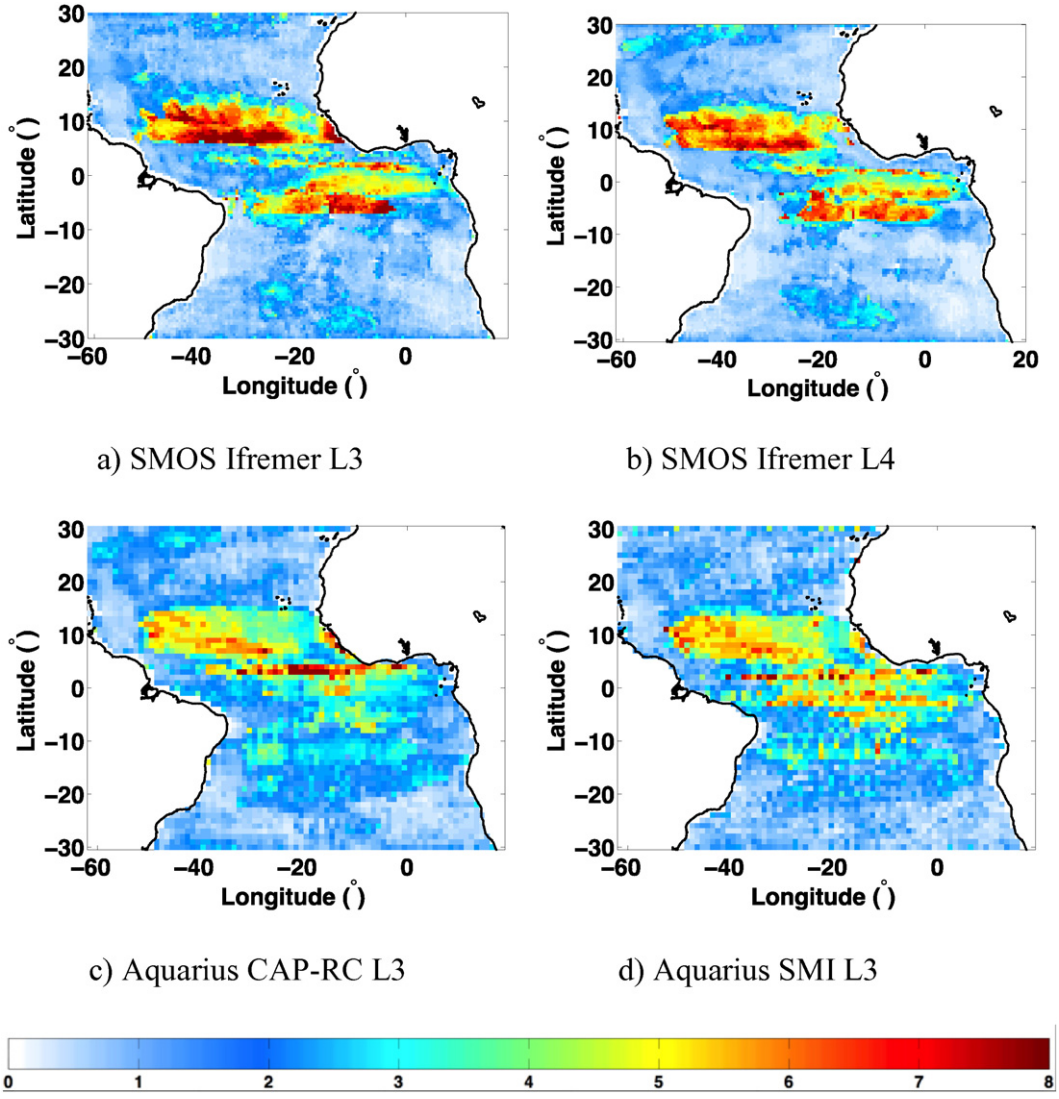

Fig. 3. Ratio of zonal to meridional decorrelation scales of SSS mean field obtained from the a) SMOS Ifremer L3, b) SMOS Ifremer L4, c) Aquarius CAP-RC L3 and d) Aquarius SMI L3 products.

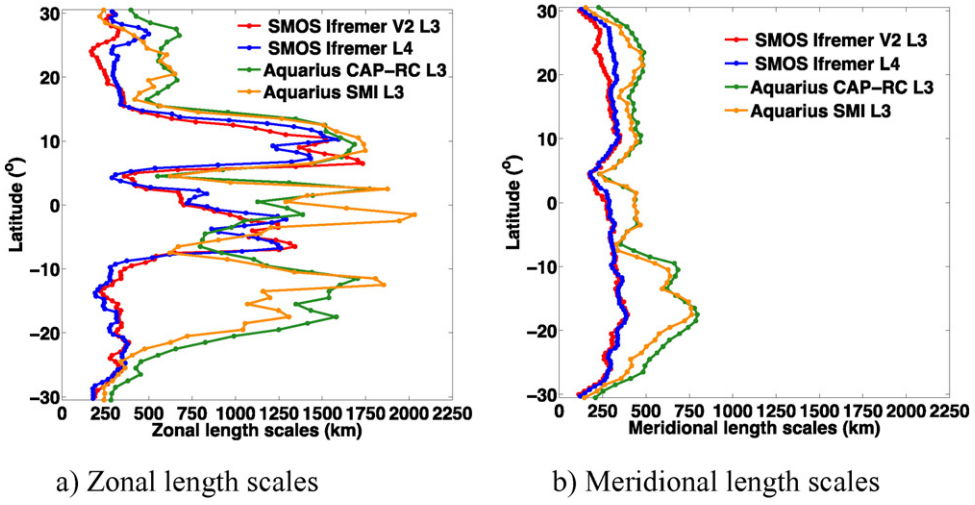

Fig. 4. The zonal averages of the a) zonal and b) meridional decorrelation scales of the SSS mean field from the SMOS Ifremer L3 (red), SMOS Ifremer L4 (blue), Aquarius CAP-RC L3 (green) and Aquarius SMI L3 (orange) products.

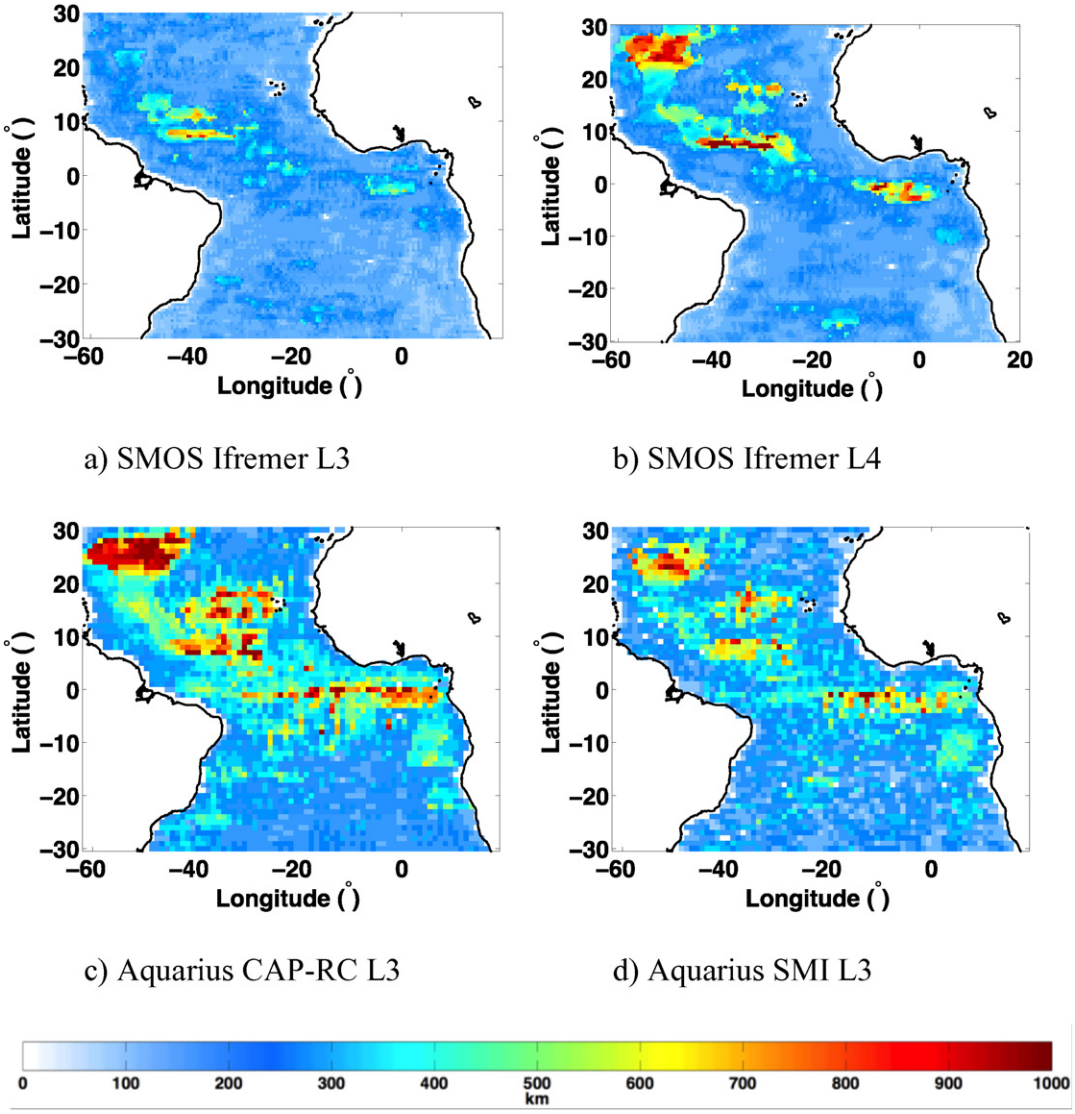

Fig. 5. The zonal spatial decorrelation scales of the SSS anomaly field (in km), derived from the a) SMOS Ifremer L3, b) SMOS Ifremer L4, c) Aquarius CAP-RC L3 and d) Aquarius SMI L3 products.

features along the southern basin coasts which are not seen in the SMOS data (Fig. 5c and d).

In turn, long meridional length scales of SSS anomalies exceeding ~400 km dominate most of the Atlantic basin in the Aquarius data (Fig. 6c and d), except in the Tropical band (3°N–10°N). Some of the same features are also visible in the SMOS Ifremer L4 data, albeit with a more patchy appearance, and are not discernible at all in the SMOS Ifremer L3. Interestingly, the removal of the seasonal cycle leaves similar or slightly longer zonal and meridional spatial scales in the Southern Sargasso Sea for the SSS anomalies as it did for the SSS mean field, this region now standing out clearly in all products except SMOS Ifremer L3 (Figs. 5 and 6b–d). The less dynamic conditions of the Sargasso Sea regime lead to SSS anomalies being correlated over length scales that exceed ~1000 km in the zonal direction and reach up to ~700–900 km in the meridional direction.

As shown in Fig. 4 for the SSS mean field, Fig. 8 summarizes the zonal and meridional spatial scales of the SSS anomaly field over the Tropical Atlantic basin 30°N–30°S in the form of zonal averages, making it easy to observe the larger decorrelation length scales of the Aquarius L3 products. Despite the difference in magnitude between SMOS and Aquarius, there is however good consistency now between the different products in the latitudinal distribution of both the zonal and meridional scales. All products place a peak in zonal length scales of SSS anomalies at ~10°N (Fig. 8a), as was also the case for the SSS mean field (Fig. 4a). However, whereas SMOS and Aquarius previously indicated double-peaks for the SSS mean field at 5°S and the Equator respectively, here, all products point to a second single peak at the Equator, except for SMOS Ifremer L3 which has no second peak. The large discrepancy in zonal length scales previously observed in the South Atlantic (Fig. 4a) also vanishes when considering SSS anomalies. Similarly, the meridional length scales show good agreement in latitudinal distribution for all four products, with a notably excellent correspondence also in the magnitude of the scales between the Aquarius SMI L3 and SMOS Ifremer L4 products (Fig. 8b).

3.3. Temporal decorrelation scales of the SSS mean and anomaly fields

As for the spatial scales, the temporal decorrelation scales of SSS are examined successively for the mean field and the anomaly field without the seasonal cycle. Fig. 9 displays the temporal scales of the SSS mean field, indicating similar overall patterns among the four datasets, albeit appearing more clearly delineated in the SMOS products. The longest persistence in time is observed in the Southern Sargasso Sea, where it reaches up to 190 days (beyond the range of the color bar scale). Once

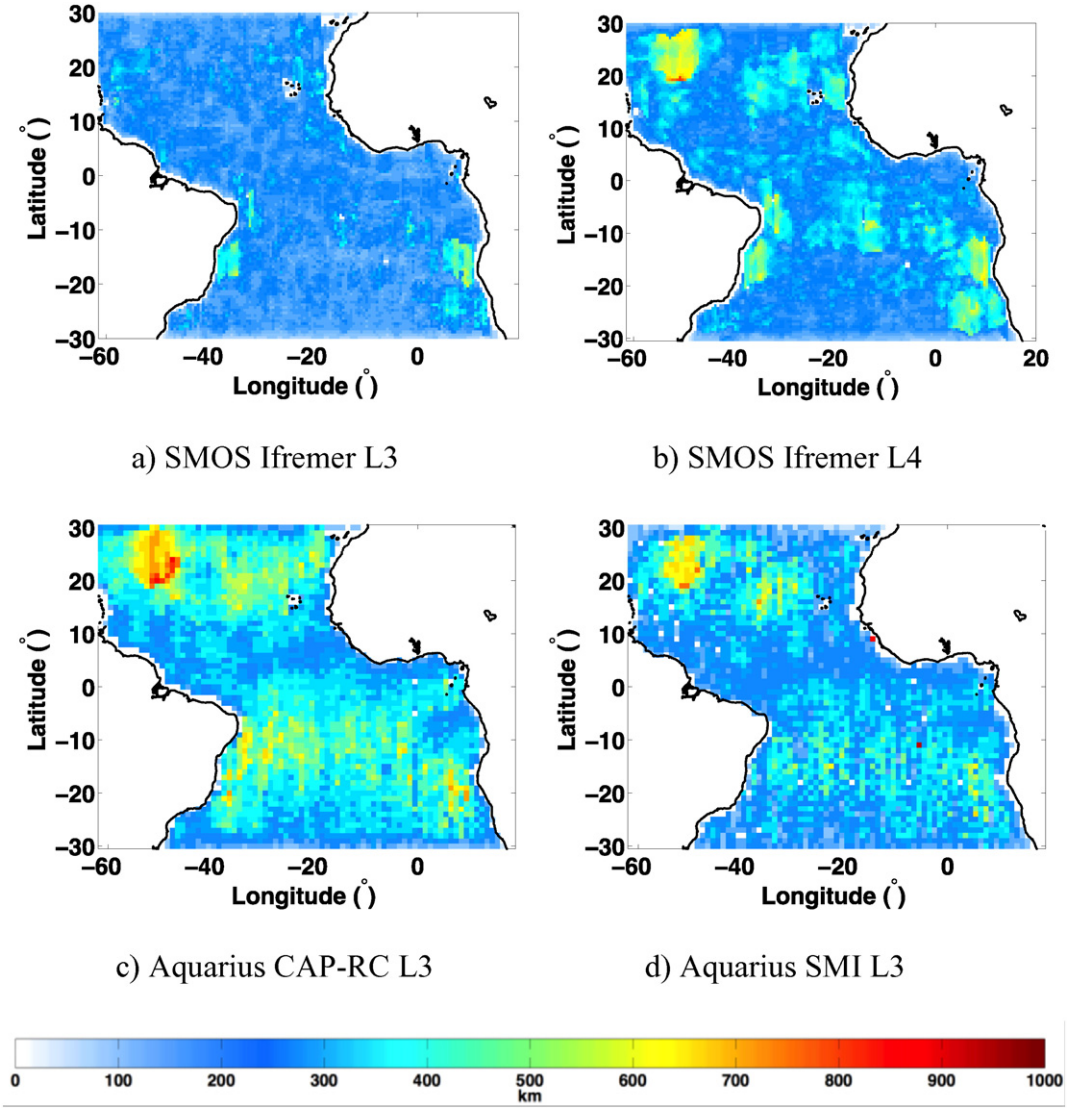

Fig. 6. The meridional spatial decorrelation scales of the SSS anomaly field (in km), derived from the a) SMOS Ifremer L3, b) SMOS Ifremer L4, c) Aquarius CAP-RC L3 and d) Aquarius SMI L3 products.

again, this feature is seen in all products except the SMOS Ifremer L3. Other longer-lived features with decorrelation times around 60–80 days, occur in the Caribbean Current region, the North and South Tropics, the East Equatorial region, and in the vicinity of the Angola Dome and Angola Current. Both Aquarius products also place a very long-lived feature (>100 days) off the coast of Namibia in the South Atlantic.

Zonal averages of the temporal decorrelation scales of the mean SSS field are shown in Fig. 11, and indicate that SMOS and Aquarius products generally report similar decorrelation times except in the South Atlantic (~10°S–25°S) (Fig. 11a). Interestingly, SMOS Ifremer L3 data suggest generally longer temporal scales (~10 days longer) than SMOS Ifremer L4, particularly southward of 10°N (Fig. 11a).

Fig. 10 shows the temporal decorrelation scales of the SSS anomaly field. Removing the seasonal cycle reduces significantly the temporal persistence of the SSS anomaly field over most of the basin, which is now typically ~20–30 days, except in a few localized areas. Notable decreases are those observed in the North and South Tropics and the East Equatorial Atlantic region.

In contrast, the long decorrelation time previously noted in the SSS mean field in the South Sargasso Sea is still visible, and continues to dominate the region with temporal scales for the SSS anomalies of up to ~200 days (well beyond the range of the color bar scale shown in Fig. 10). Once again, this feature is seen clearly in all products except the SMOS Ifremer L3 data. Other long-persistence features in SSS anomalies are observed in a cluster centred around 15°N, 35°W (~70–90 days) and in the Caribbean Current region (~40–50 days). Finally, Aquarius suggests several long temporal persistence features along the African coast, particularly in the Gulf of Guinea, at 10°S close to the Angola Dome (Fig. 10, c and d), and off the coast of Namibia, towards the southern part of the Angola-Benguela Front (~16°S). As these are not observed in either of the Ifremer SMOS products, and occur in a region known for Radio Frequency Interference (RFI) issues, these could point to some residual RFI contamination in the Aquarius data in this area.

The zonal averages of the temporal scales for the SSS anomalies shown in Fig. 11b confirm the general reduction in time persistence across the basin compared to the SSS mean field, except for latitudes north of 20°N affected by the long decorrelation time of the Sargasso Sea. There is generally good correspondence between the different datasets, including an excellent agreement at ~24°N between the SMOS Ifremer L4 and Aquarius CAP-RC L3 data. The one exception is the SMOS Ifremer L3 product which gives lower estimates of the time persistence north of 20°N and higher estimates of it by 10 days everywhere else. We note however that southwards of the Equator the SSS

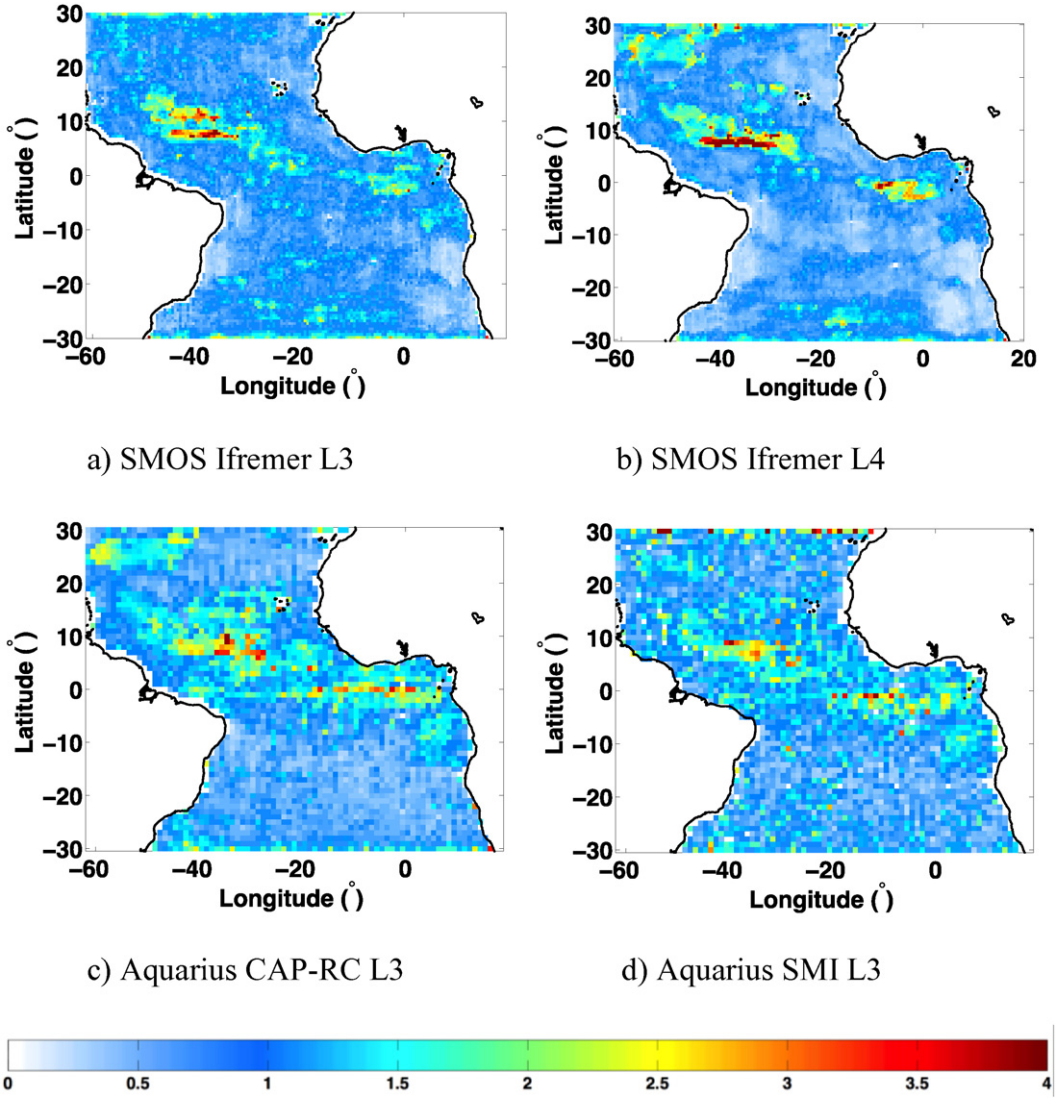

Fig. 7. The ratio of zonal to meridional decorrelation scales of the SSS anomaly field obtained from the a) SMOS Ifremer L3, b) SMOS Ifremer L4, c) Aquarius CAP-RC L3 and d) Aquarius SMI L3 products.

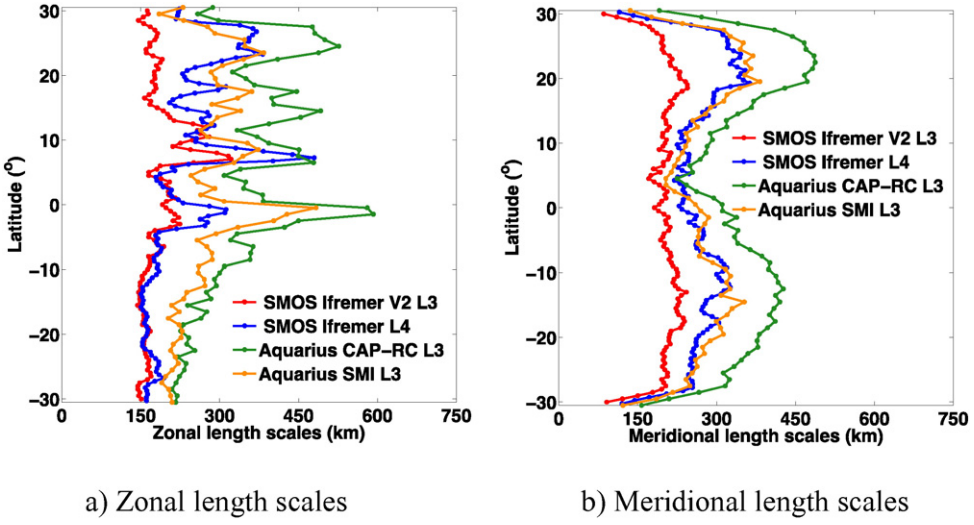

Fig. 8. The zonal averages of a) the zonal and b) the meridional decorrelation scales of the SSS anomaly field from the SMOS Ifremer L3 (red), SMOS Ifremer L4 (blue), Aquarius CAP-RC L3 (green) and Aquarius SMI L3 (orange) products.

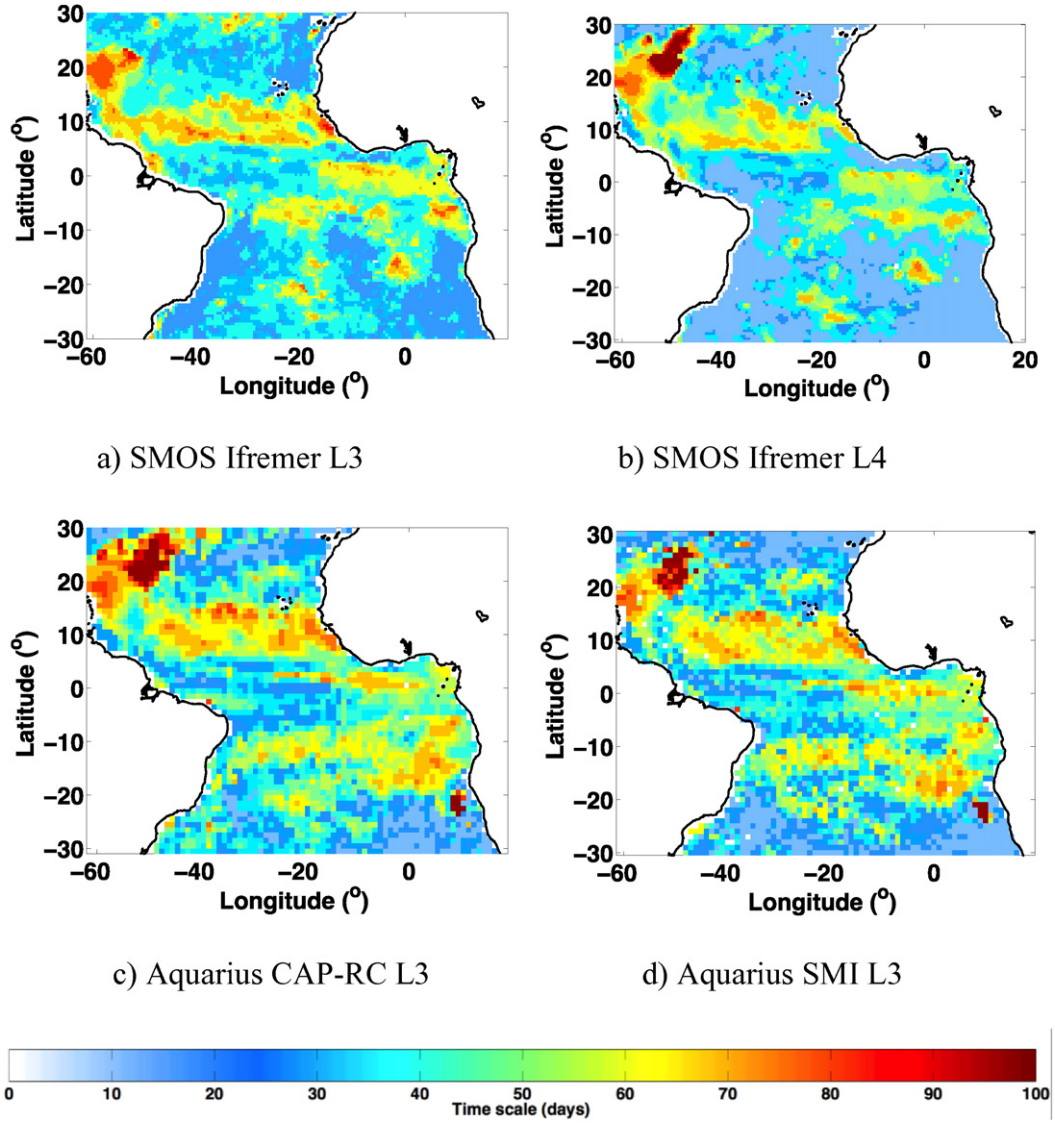

Fig. 9. The temporal decorrelation scales of the SSS mean field (in days) derived from the a) SMOS Ifremer L3, b) SMOS Ifremer L4, c) Aquarius CAP-RC L3 and d) Aquarius SMI L3 products.

anomaly field is characterized by very short temporal scales around 15–25 days, which are close to the limit of what can be determined given the temporal resolution of the products.

4. Discussion

The characteristic spatial and temporal scales of variability of the SSS mean field and the SSS anomaly field were determined from three complete years (2012–2014) of SMOS and Aquarius satellite data in the Atlantic basin 30°N–30°S. Maps of spatial and temporal decorrelation scales show significant variations with latitude and longitude, pointing to the influence of different processes and controlling mechanisms in different regions of the Atlantic basin (given that the dependence of a variable can arise both from itself and the factors that influence it, e.g. Dale & Fortin, 2009). Our analyses indicate that the characteristic spatial decorrelation scales of the SSS mean field are strongly anisotropic over parts of the Tropical Atlantic, with maps of the zonal/meridional ratio highlighting areas of strong anisotropy with unprecedented detail (Fig. 3; Fig. 7). The anisotropy of the decorrelation length scales is in agreement with previous studies based on in situ data (e.g. Delcroix et al., 2005; Reverdin et al., 2007). However, in contrast to these earlier studies, the decorrelation lengths reported by the satellite data used in this study are larger (of order 1000–2000 km for the SSS mean field) than those obtained from *in situ* measurements (of order ~200–500 km). Possible causes for this disagreement include differences in length scale estimation methods as well as differences in the space/time sampling of the SSS data. Further analyses will be needed in future to confirm whether this is the case. It is clear however that the spatial and temporal resolution of the satellite products used here (0.5°–1.0°; 7–10 days) means the satellite data cannot capture very short spatial and temporal variability in SSS, which might however affect the *in situ* measurements. For instance, Delcroix et al. (2005) use quasi-zonal and quasi-meridional SSS data along ship tracks to calculate the decorrelation length of SSS. Correlation is calculated for each degree of latitude against SSS at all other latitudes and the meridional decorrelation length is defined as the distance to the smallest computed correlation value to the north or the south. Reverdin et al. (2007), based on monthly, 1° binned *in situ* measurements from ships, floats and moorings corresponding to different depths between 2 m and >15 m, fit an exponential function to estimate the scales and limit their correlations to up to 7°, which similarly, may result in shorter spatial scales. Melnichenko et al. (2014) find much shorter meridional scales of SSS in the Atlantic 0°-40°N of the order of ~180 km between 0°–10°N and ~150 km at 30°–40°N, based on Aquarius L2 ground-track segments of 10° latitude, which likely do not smooth out some of the small scale SSS variability as compared to the L3 composite products.

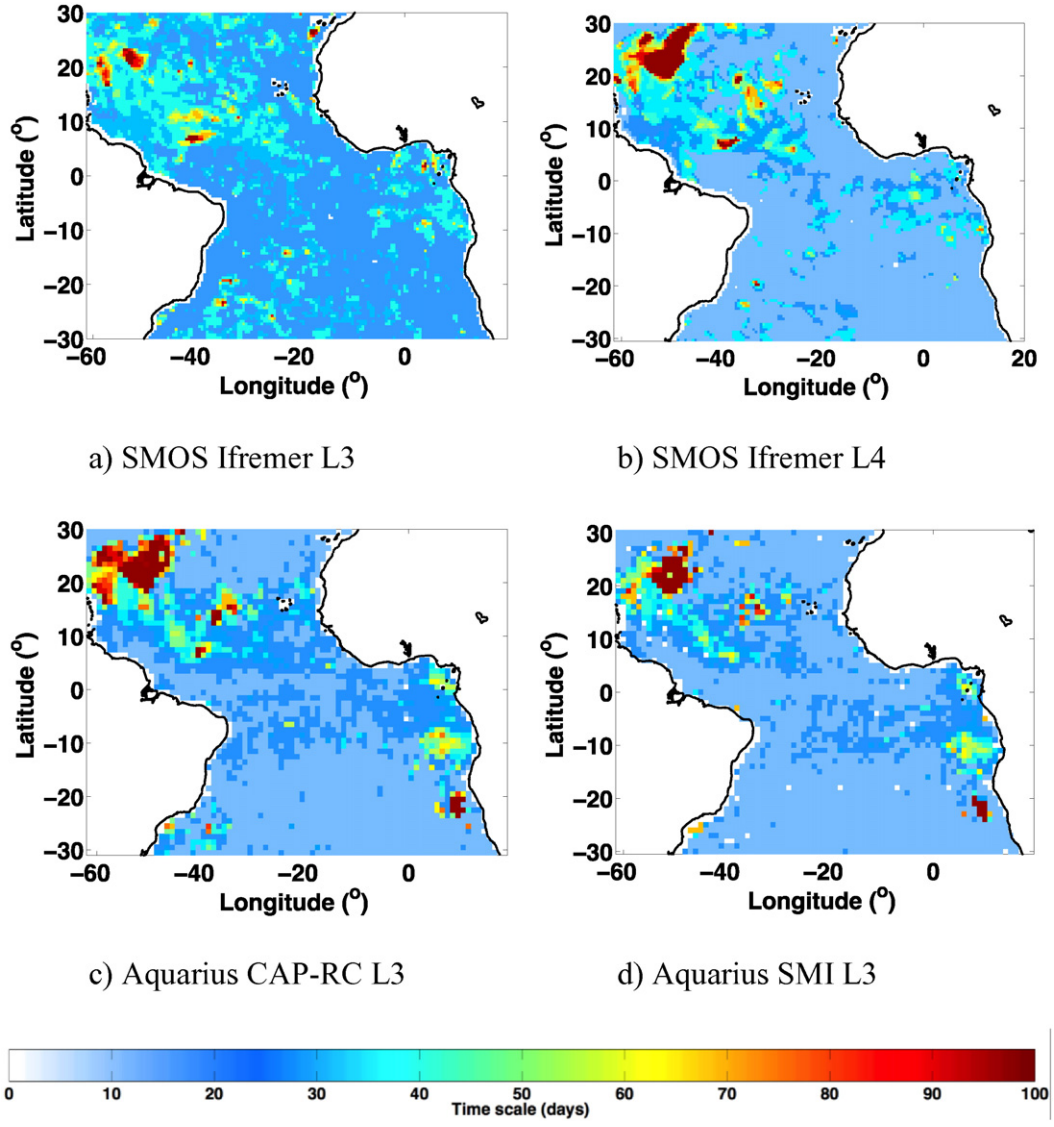

Fig. 10. The temporal scales of the SSS anomaly field (in days) derived from the a) SMOS Ifremer L3, b) SMOS Ifremer L4, c) Aquarius CAP-RC L3 and d) Aquarius SMI L3 products.

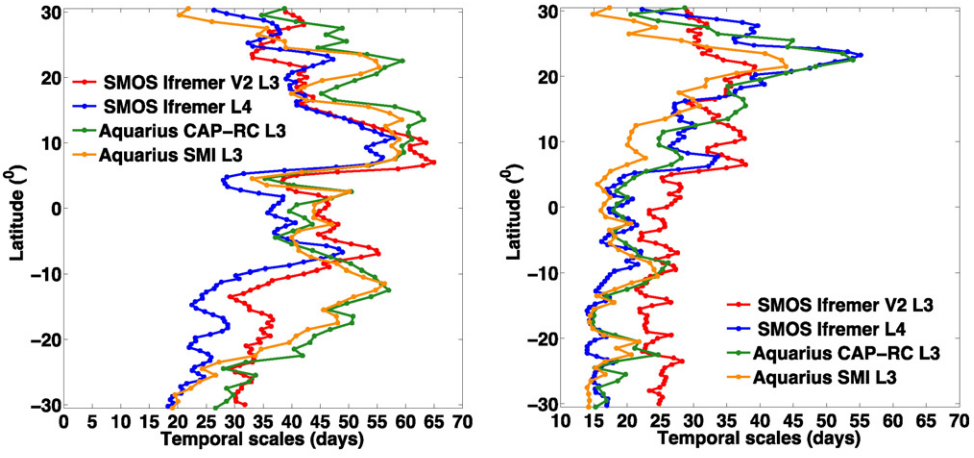

Fig. 11. The zonal averages of the temporal decorrelation scales for the SSS a) mean field and b) anomaly field, derived from the SMOS Ifremer L3 (red), SMOS Ifremer L4 (blue), Aquarius CAP-RC L3 (green) and Aquarius SMI L3 (orange) products.

The decorrelation lengths we find are also larger than estimates obtained recently with daily high-resolution ocean model output. Sena Martins, Serra, and Stammer (2015) estimate the spatio-temporal scales of SSS in the Atlantic basin between 80°N–33°S based on daily data from an eddy-resolving general circulation model with 4 km spatial resolution. The decorrelation scales they find generally reach up to ~200 km in the zonal direction and ~100 km in the meridional direction, and thus, are noticeably shorter than our estimates. Sena Martins et al. (2015) limit their search radius to ~160 km in the Tropics and ~100 km further north, which could contribute to their finding shorter length scales, in addition to other differences in the methodology applied, the relaxation of the model to the climatology and associated regional biases. However, we hypothesise here that the fine temporal and spatial resolution of the model data make it possible to resolve small scale spatial gradients and higher-frequency temporal variability of the SSS field, which, Sena Martins et al. (2015) point out, are likely to be linked to eddy-related activity and fast atmospheric processes. These same processes cannot be resolved with the satellite SSS L3 and L4 products used in our study (0.5°–1.0°; 7–10 days). One way to verify this hypothesis would be to apply our estimation method to ocean model products with the same spatio-temporal resolution as the satellite SSS products used here. However, such extensive additional analyses are beyond the scope of the present paper.

The second major outcome of our work is the impact of removing the seasonal cycle from the SSS data. This results in a marked change in spatial distribution and a notable decrease in magnitude of both the spatial and temporal decorrelation scales over most of the basin. The impact is particularly evident for zonal length scales in the Tropics, where the variability of the SSS mean field is dominated by strongly seasonal effects that decorrelate over ~60–80 days and occur over large zonal scales. These are consistent with processes linked to atmosphere/ocean exchanges such as the migration of the ITCZ. While lengths scales are generally much smaller for the SSS anomalies, relatively large zonal scales are nevertheless still visible in the SSS anomaly field in small parts of the basin, particularly in the Northern Tropics and the East Equatorial basin. These stand out clearly as regions of strong anisotropy in the SSS anomaly field (Fig. 7) and are associated with relatively short temporal decorrelation (Fig. 10), pointing to the possible influence of advection by zonal ocean currents. In the Western Equatorial Atlantic, short spatial and temporal scales associated with low anisotropy are consistent with very dynamic eddy activity in the vicinity of river discharge from the Amazon and Orinoco rivers, advection by the North Brazilian Current (NBC), the North Equatorial Counter Current (NECC) and equatorial upwelling. In contrast, the large temporal and spatial decorrelation lengths and low anisotropy observed in the N.W. part of the basin are consistent with the slow gyre circulation of the Sargasso Sea.

Comparison of the spatial and temporal length scales derived from the different satellite SSS products reveals broad agreement in the results, with some notable exceptions. The largest difference between SMOS and Aquarius products occurs in the South Atlantic, where both Aquarius SMI and CAP-RC products suggest significantly longer spatial scales than SMOS over most of the Southern basin. The disagreement is very prominent in the zonal and meridional scales of the SSS mean field, but less so in the SSS anomaly field and in the temporal scales reported by the two satellites. While this suggests that the source of this dissimilarity has a seasonal component, the reason is unknown. Although beyond the scope of this paper, an initial cursory examination of the spatial scales of SSS in the Pacific does not reveal a similar pattern of long spatial decorrelation lengths from Aquarius over the southern part of the Pacific region. Further investigation is required to unravel the different behaviour between SMOS and Aquarius missions in the Southern Atlantic basin and their associated characteristics.

Moreover, possible sources of differences between the Aquarius and SMOS results include factors influencing the accuracy of satellite SSS measurements, such as contamination by land, which can bias SSS observations close to coast and up to 1500 km away from land in the case of SMOS. This can result in too fresh signals (e.g. Reul et al., 2012b) and the introduction of artificial SSS variability (Hernandez et al., 2014). Likewise, errors in SSS linked to imperfect mitigation of strong radio-frequency interference (RFI) could also introduce non-geophysical variability in the satellite SSS. This is the case particularly in regions such as the N.W. Atlantic, the Gulf of Guinea and along the coast of Angola and Namibia, where some of the persistent features observed in Aquarius (but not SMOS) are likely to be linked to residual RFI effects.

Finally, differences in spatial and temporal resolution of the different satellite SSS products used in this work do not seem to play a major role in the estimated SSS variability. For example, there is occasionally remarkable agreement between the SMOS Ifremer L4 (0.5°; 7-days) and Aquarius (1°; 7-days) products (e.g. Fig. 8b; Fig. 11b). On the other hand, the SMOS Ifremer L3 products (0.5°; 10-days) give distinctly different results from other products, returning typically longer temporal scales and much smoother maps of spatial decorrelation scales, even failing at times to detect well-defined features (e.g. Sargasso Sea). The slightly coarser temporal resolution of 10-days may of course contribute to these differences, but it seems more likely that the reduced variability of the SMOS Ifremer L3 products originates from the bias correction of the SMOS satellite SSS against the static WOA01 climatology.

5. Conclusions

The spatial and temporal decorrelation scales of SSS have been estimated for the first time from satellite measurements in the Atlantic basin between 30°N and 30°S using three full years of concurrent data from the SMOS and Aquarius missions in 2012–2014. The results show that:

- The satellite SSS data return spatial scales of variability in the Tropical Atlantic that reach 2000 km zonally, and are significantly larger than earlier estimates from in situ data and a high-resolution ocean model. It is hypothesised that our larger decorrelation scales are due to the spatial and temporal resolution of the satellite products used in this study (0.5°–1.0°; 7–10 days) which prevent the satellite data from capturing short spatial and temporal variability in SSS that is seen by *in situ* measurements and high-resolution models.
- The removal of the seasonal cycle decreases noticeably the spatial and temporal decorrelation scales of SSS, although the anisotropy is still preserved in parts of the Tropics. An exception occurs in the North-Western part of our domain and in the Southern Sargasso Sea, where the SSS anomaly field displays longer spatio-temporal scales.
- The spatial decorrelation scales of SSS are strongly anisotropic in the Tropical Atlantic, displaying large zonal scales and seasonally-dominated temporal variability that are consistent with controlling mechanisms linked to atmosphere/ocean exchanges and the seasonal migration of the ITCZ. Large zonal scales in the SSS anomaly field suggest the influence of advection by zonal ocean currents in some parts of the basin. Elsewhere, isotropic scales may indicate the presence of eddies, associated with short temporal decorrelation (up to 30 days) in dynamic regions near river plumes and boundary currents.
- Overall, there is good consistency between the spatio-temporal scales estimated from the SMOS Ifremer L4 and the Aquarius L3 products despite their individual calibration characteristics, with differences in spatio-temporal resolution between the different products having little impact on the estimated SSS variability. One exception relates to SSS in the South Atlantic, where Aquarius suggests much larger zonal and meridional decorrelation scales than SMOS, for reasons that are unclear and require further investigation. The SMOS Ifremer L3 returns longer temporal decorrelation scales and smoother spatial decorrelation fields, linked to the impact of SSS bias correction against the static WOA01 climatology.

The improved description of spatio-temporal SSS decorrelation scales in the Tropical Atlantic presented here provides a valuable new resource to study and understand regional variations in the mechanisms controlling SSS variability. The spatial scales of SSS identify regions over the basin that are characterized by homogeneous SSS behaviour, while temporal variability estimates gives insight into the persistence of SSS features in time. This work has important applications for the evaluation of how to maximize the value of satellite SSS data in assimilation systems, for the development of optimally interpolated SSS products, as well as for the definition of appropriate validation procedures of the various satellite SSS products.

To conclude, a new era for oceanography has started with satellite salinity missions such as SMOS, Aquarius and SMAP, which provide new knowledge and unprecedented detail about the variability and controlling mechanisms of SSS. The approach presented in the paper represents a very powerful new investigative tool that is equally applicable to SSS in other regions of the globe, to other SSS products and to other ocean geophysical properties. Future plans include applying this approach to ocean model data to explore the possible reasons for the very long scales we found. So far, only three full years of concurrent data from the two missions were available, and the estimation should be repeated once longer time series are available, emphasizing the necessity of ensuring the continuity of remotely-sensed SSS measurements from satellites in the future. Further analysis of the growing satellite data record in combination with *in situ* observations and models will improve our interpretation of the SSS variability and its relation with atmospheric forcing and horizontal and vertical oceanic processes, to provide a comprehensive, three dimensional representation of the global salinity field and its variability.

Acknowledgements

We acknowledge the European Space Agency (ESA) and the Support To Science Element (STSE) SMOS and Surface Ocean Salinity (SMOS + SOS) project, for providing the funding to support this research. We also thank the UK Natural Environment Research Council National Capability for co-funding M. Srokosz, C. Gommenginger and S. Josey. The SMOS Ifremer L3 and L4 products were provided by the Centre Aval de Traitement des Données SMOS Expertise Center-Ocean Salinity (CATDS-CECOS, www.catds.fr), while the Aquarius SMI and CAP-RC L3 products from the US National Aeronautics and Space Administration (NASA)'s Physical Oceanography Distributed Active Archive Center (PODAAC) and Jet Propulsion Laboratory (http://podaac.jpl.nasa.gov). Finally, we are also thankful to members of the Marine Physics and Ocean Climate (MPOC) and Marine Systems Modelling (MSM) Groups at the National Oceanography Centre Southampton for their assistance in optimizing the programming code used in this project.

References

Banks, C. J., Gommenginger, C. P., Srokosz, M. A., & Snaith, H. M. (2012). Validating SMOS ocean surface salinity in the Atlantic with Argo and operational ocean model data. *IEEE Transactions on Geoscience and Remote Sensing*, *50*(5), 1688–1702. http://dx.doi.org/10.1109/TGRS.2011.2167340.

Boutin, J., Martin, N., Yin, X., Font, J., Reul, N., & Spurgeon, P. (2012). First assessment of SMOS data over open ocean: Part II—Sea surface salinity. *IEEE Transactions on Geoscience and Remote Sensing*, *50*(5), 1662–1675. http://dx.doi.org/10.1109/TGRS.2012.2184546.

Boutin, J., Martin, N., Reverdin, G., Yin, X., & Gaillard, F. (2013). Sea surface freshening inferred from SMOS and ARGO salinity: impact of rain. *Ocean Science*, *9*(1), 183–192. http://dx.doi.org/10.5194/os-9-183-2013.

Boutin, J., Martin, N., Reverdin, G., Morisset, S., Yin, X., Centurioni, L., & Reul, N. (2014). Sea surface salinity under rain cells: SMOS satellite and in situ drifters observations. *Journal of Geophysical Research, Oceans*, *119*, 5533–5545. http://dx.doi.org/10.1002/2014JC010070.

Brown, M. E., Escobar, V., Moran, S., Entekhabi, D., O'Neill, P. E., Njoku, E. G., ... Entin, J. K. (2013). NASA's soil moisture active passive (SMAP) mission and opportunities for applications users. *Bulletin of the American Meteorological Society*, *94*, 1125–1128. http://dx.doi.org/10.1175/BAMS-D-11-00049.1.

Dale, M. R. T., & Fortin, M. -J. (2009). Spatial autocorrelation and statistical tests: Some solutions. *Journal of Agricultural, Biological, and Environmental Statistics*, *14*(2), 188–206. http://dx.doi.org/10.1198/jabes.2009.0012.

Delcroix, T., McPhaden, M. J., Dessier, A., & Gouriou, Y. (2005). Time and space scales for sea surface salinity in the tropical oceans. *Deep Sea Research Part I: Oceanographic Research Papers*, *52*(5), 787–813. http://dx.doi.org/10.1016/j.dsr.2004.11.012.

Foltz, G. R., & McPhaden, M. J. (2008). Seasonal mixed layer salinity balance of the tropical North Atlantic Ocean. *Journal of Geophysical Research*, *113*, C02013. http://dx.doi.org/10.1029/2007JC004178.

Hackert, E., Busalacchi, A. J., & Ballabrera-Poy, J. (2014). Impact of Aquarius sea surface salinity observations on coupled forecasts for the tropical Indo-Pacific Ocean. *Journal of Geophysical Research, Oceans*, *119*, 4045–4067. http://dx.doi.org/10.1002/2013JC009697.

Hasson, A., Delcroix, T., & Boutin, J. (2013). Formation and variability of the South Pacific Sea Surface Salinity maximum in recent decades. *Journal of Geophysical Research, Oceans*, *118*(10), 5109–5116. http://dx.doi.org/10.1002/jgrc.20367.

Henocq, C., Boutin, J., Reverdin, G., Petitcolin, F., Arnault, S., & Lattes, P. (2010). Vertical variability of near-surface salinity in the tropics: Consequences for L-band radiometer calibration and validation. *Journal of Atmospheric and Oceanic Technology*, *27*(1), 192–209. http://dx.doi.org/10.1175/2009JTECHO670.1.

Hernandez, O., Boutin, J., Kolodziejczyk, N., Reverdin, G., Martin, N., Gaillard, F., ... Vergely, J. L. (2014). SMOS salinity in the subtropical North Atlantic salinity maximum: 1. Comparison with Aquarius and in situ salinity. *Journal of Geophysical Research, Oceans*, *119*. http://dx.doi.org/10.1002/2013JC009610.

Hoareau, N., Umbert, M., Martínez, J., Turiel, A., & Ballabrera-Poy, J. (2014). On the potential of data assimilation to generate SMOS-Level 4 maps of sea surface salinity. *Remote Sensing of Environment*, *146*, 188–200. http://dx.doi.org/10.1016/j.rse.2013.10.005.

Kerr, Y., Waldteufel, J. -P., Boutin, J., Escorihuela, M. -J., Font, J., Reul, N., ... Mecklenburg, S. (2010). The SMOS mission: New tool for monitoring key elements of the global water cycle. *Proceedings of the IEEE*, *98*(5), 666–687.

Köhl, A., Martins, M. S., & Stammer, D. (2014). Impact of assimilating surface salinity from SMOS on ocean circulation estimates. *Journal of Geophysical Research, Oceans*, *119*, 5449–5464. http://dx.doi.org/10.1002/2014JC010040.

Lagerloef, G., Colomb, F. R., Vine, D. L., Wentz, F., Yueh, S., Ruf, C., ... Swift, C. (2008). The Aquarius/SAC-D mission: Designed to meet the salinity remote-sensing challenge. *Oceanography*, *21*(1), 68–81.

Lagerloef, G., et al. (2013), Aquarius data release V2.0 validation analysis, Aquarius Proj. Doc. AQ-014-PS-0016. [Available at ftp://podaac-ftp. jpl.nasa.gov/allData/aquarius/docs/v2/AQ-014-PS-0016_AquariusSalinityDataValidationAnalysis_DatasetVersion2.0.pdf.]

Lee, T., Lagerloef, G., Gierach, M. M., Kao, H. -Y., Yueh, S., & Dohan, K. (2012). Aquarius reveals salinity structure of tropical instability waves. *Geophysical Research Letters*, *39*, L12610. http://dx.doi.org/10.1029/2012GL052232.

Lukas, R., & Lindstrom, E. (1991). The mixed layer of the western equatorial Pacific Ocean. *Journal of Geophysical Research*, *96*(suppl), 3343–3357.

Mecklenburg, S., Drusch, M., Kerr, Y., Font, J., Martin-Neira, M., Delwart, S., ... Crapolicchio, R. (2012). ESA's soil moisture and ocean salinity mission: Mission performance and operations. *IEEE Transactions on Geoscience and Remote Sensing*, *50*(5), 1354–1366.

Melnichenko O., P. Hacker, N. Maximenko, G. Lagerloef, and J. Potemra (2014), Spatial optimal interpolation of Aquarius sea surface salinity: Algorithms and implementation in the North Atlantic. Journal of Atmospheric and Oceanic Technology, 31, 1583–1600. http://dx.doi.org/10.1175/JTECH-D-13-00241.1.

Menezes, V. V., Vianna, M. L., & Phillips, H. E. (2014). Aquarius sea surface salinity in the South Indian Ocean: Revealing annual-period planetary waves. *Journal of Geophysical Research, Oceans*, *119*, 3883–3908. http://dx.doi.org/10.1002/2014JC009935.

Reul & Ifremer CATDS-CECOS Team (2012). *SMOS L3 SSS Research products: Product user manual, reprocessed year 2010–2012: IFREMER, Plouzané, France.*

Reul, N., Tenerelli, J., Boutin, J., Chapron, B., Paul, F., Brion, E., ... Archer, O. (2012b). Overview of the first SMOS Sea surface salinity products. Part I: Quality assessment for the second half of 2010. *IEEE Transactions on Geoscience and Remote Sensing*, *50*(5), 1636–1647. http://dx.doi.org/10.1109/TGRS.2012. 2188408.

Reul, N., Fournier, S., Boutin, J., Hernandez, O., Maes, C., Chapron, B., ... Delwart, S. (2013). Sea surface salinity observations from space with the SMOS satellite: A new means to monitor the marine branch of the water cycle. *Surveys in Geophysics*. http://dx.doi.org/10.1007/s10712-013-9244-0.

Reul & Tenerelli (2015). *SMOS level 3 & 4 research products of the centre d' expertise Ifremer du CATDS: Algorithm theoretical background document: IFREMER, Plouzané, France.*

Reverdin, G., Kestenare, E., Frankignoul, C., & Delcroix, T. (2007). Surface salinity in the Atlantic Ocean (30°S–50°N). *Progress in Oceanography*, *73*, 311–340. http://dx.doi.org/10.1016/j.pocean.2006.11.004.

Schmitt, R. (2008). Salinity and the global water cycle. *Oceanography*, *21*(1), 12–19.

Sena Martins, M., Serra, N., & Stammer, D. (2015). Spatial and temporal scales of sea surface salinity variability in the Atlantic Ocean. *Journal of Geophysical Research, Oceans*. http://dx.doi.org/10.1002/2014JC010649 Accepted Author Manuscript.

Tang, W., Yueh, S. H., Fore, A. G., Hayashi, A., Lee, T., & Lagerloef, G. (2014). Uncertainty of Aquarius sea surface salinity retrieved under rainy conditions and its implication on the water cycle study. *Journal of Geophysical Research, Oceans*, *119*, 4821–4839. http://dx.doi.org/10.1002/2014JC009834.

Tang, W., Yueh, S. H., Fore, A. G., & Hayashi, A. (2014). Validation of Aquarius sea surface salinity with in situ measurements from Argo floats and moored buoys. *Journal of Geophysical Research, Oceans*, *119*, 6171–6189. http://dx.doi.org/10.1002/2014JC010101.

Tzortzi, E., Josey, S. A., Srokosz, M., & Gommenginger, C. (2013). Tropical Atlantic salinity variability: New insights from SMOS. *Geophysical Research Letters*, *40*, 1–5. http://dx.doi.org/10.1002/grl.50225.

Tzortzi, E. (2015). *Sea surface salinity in the Atlantic Ocean from the SMOS mission and its relation to Freshwater fluxes*. University of Southampton, School of Ocean and Earth Science Doctoral Thesis, 224pp.

Van den Dool, H., Peng, P., Johansson, A., Chelliah, M., Shabbar, A., & Saha, S. (2006). Seasonal-to-decadal predictability and prediction of North American climate—The Atlantic influence, J. *Climate*, *19*, 6005–6024.

Vellinga, M., & Wu, P. (2004). Low-latitude freshwater influence on centennial variability of the Atlantic thermohaline circulation. *Journal of Climate*, *17*, 4498–4511.

Vernieres, G., Kovach, R., Keppenne, C., Akella, S., Brucker, L., & Dinnat, E. (2014). The impact of the assimilation of Aquarius sea surface salinity data in the GEOS ocean data assimilation system. *Journal of Geophysical Research, Oceans*, *119*, 6974–6987. http://dx.doi.org/10.1002/2014JC010006.

Vinogradova, N., Ponte, R. M., Fukumori, I., & Wang, O. (2014). Estimating satellite salinity errors for assimilation of Aquarius and SMOS data into climate models. *Journal of Geophysical Research, Oceans*, *119*, 4732–4744. http://dx.doi.org/10.1002/2014JC009906.

Wentz, F., S. Yueh, and G. Lagerloef (2014), Aquarius Official Release Level 3 Sea Surface Salinity Standard Mapped Image 7-Day Data V3.0. Ver. 3.0. PO.DAAC, CA, USA. Dataset accessed [2015-04-22] at http://dx.doi.org/10.5067/AQUAR-3S7PS.

Yueh, S. H., & Chaubell, J. (2012). Sea surface salinity and wind retrieval using combined passive and active L-band microwave observations. *IEEE Transactions on Geoscience and Remote Sensing*, *50*(4), 1022–1032.

Yueh, S. H., Tang, W., Fore, A., Neumann, G., Hayashi, A., Freedman, A., ... Lagerloef, G. (2013). L-band passive and active microwave geophysical model functions of ocean surface winds and applications to Aquarius retrieval. *IEEE Transactions on Geoscience and Remote Sensing*, *51*(9), 4619–4632. http://dx.doi.org/10.1109/TGRS.2013.2266915.

Yueh, S. H., Tang, W., Fore, A., Hayashi, A., & Song, Y. (2014). Aquarius geophysical model function and combined active passive algorithm for ocean surface salinity and wind retrieval. *Journal of Geophysical Research, Oceans*, *119*, 5360–5379. http://dx.doi.org/10.1002/2014JC009939.